NASA TECHNICAL NOTE

NASA TN D-2548

NASA TN D-2548

RELATION OF EMITTED ULTRAVIOLET RADIATION TO COMBUSTION OF HYDROGEN AND OXYGEN AT 20 ATMOSPHERES

by Marshall C. Burrows and Ronald Razner

Lewis Research Center
Cleveland, Ohio

NATIONAL AERONAUTICS AND SPACE ADMINISTRATION • WASHINGTON, D. C. • DECEMBER 1964

RELATION OF EMITTED ULTRAVIOLET RADIATION TO COMBUSTION OF HYDROGEN AND OXYGEN AT 20 ATMOSPHERES

By Marshall C. Burrows and Ronald Razner

Lewis Research Center
Cleveland, Ohio

NATIONAL AERONAUTICS AND SPACE ADMINISTRATION

For sale by the Office of Technical Services, Department of Commerce,
Washington, D.C. 20230 -- Price $1.00

RELATION OF EMITTED ULTRAVIOLET RADIATION TO COMBUSTION OF HYDROGEN AND OXYGEN AT 20 ATMOSPHERES

by Marshall C. Burrows and Ronald Razner

Lewis Research Center

SUMMARY

Emitted radiation from the combustion of gaseous hydrogen and liquid oxygen was measured in the spectral range from 2500 to 4500 angstroms. Pressure in the combustion chamber was maintained at approximately 20 atmospheres.

The hydroxyl radical (OH) emitted strongly in the region between 2500 and 3500 angstroms. Principal molecular oxygen (O_2) emission extended from 3000 to 4000 angstroms. Background or continuum radiation extended throughout the observed spectral range.

Analysis of radiation from the OH radical showed that OH was in thermal equilibrium with its surroundings, in both the reaction zone and in the mixed products of reaction. Radiating OH and O_2 lines were severely self-absorbed in all bands because of the cool combustor boundaries and gas mixtures with non-uniform temperature profiles.

In general, radiation intensity measurements showed that it was possible to detect variations in the oxidant-fuel weight ratio within the combustion chamber on both a time-averaged and a time-resolved basis. The axial distance required for complete combustion and mixing of the products was determined for several injector types over a range of oxidant-fuel ratios. A description of the combustion zone based on a constant-temperature reaction with subsequent mixing of the products with the excess propellant was consistent with the measurements.

INTRODUCTION

One of the few methods that can be used to study the combustion characteristics of liquid-oxygen jets reacting in a hydrogen (H_2) atmosphere involves observation of the emitted radiation. This radiation is produced by thermal or chemiluminescent excitation of various molecules and radicals in the combustion zone. Extensive studies on hydrogen-oxygen (H_2-O_2) flames at low pressure have shown that radiation occurs in the ultraviolet and visible spectrum because of the hydroxyl radical (OH) and oxygen (O_2), and in the red-infrared

spectrum because of OH and water vapor (H_2O) (ref. 1). When the radiation is thermally excited, it is possible (ref. 2) to determine concentration profiles of the various gases by absorption spectroscopy.

For quantitative measurements of radiation from the high-pressure combustion gases to be meaningful, it is necessary to know if the radiation is emitted by molecules in thermal equilibrium or if it is a chemiluminescent phenomenon. The first objective of this study was to determine whether equilibrium existed by obtaining the apparent temperatures of the radiating gases by two methods and comparing them with the computed temperatures of the products based on an equilibrium gas composition. The second objective was to relate the measured OH intensities to the state of the hydrogen-oxygen combustion at various overall mixture ratios and axial distances from the injector.

Spectral radiation measurements were made on the gases at various positions in three combustors. Total OH radiation was measured at various axial distances downstream from the injector for several oxidant-fuel weight ratios (o/f). From these measurements it was possible to determine (1) OH brightness and rotational temperatures, (2) average axial distances for complete combustion and mixing, and (3) local periodic and nonperiodic variations in the radiation brought about by nonuniform propellant flows or nonuniform mixing of products. A description of the combustion process is advanced to explain the observed behavior.

APPARATUS AND PROCEDURE

The combustor was constructed in sections (fig. 1) so that an observation window could be positioned in one of five axial locations. Since all parts were copper, uncooled runs as long as 8 seconds were possible. Three injectors

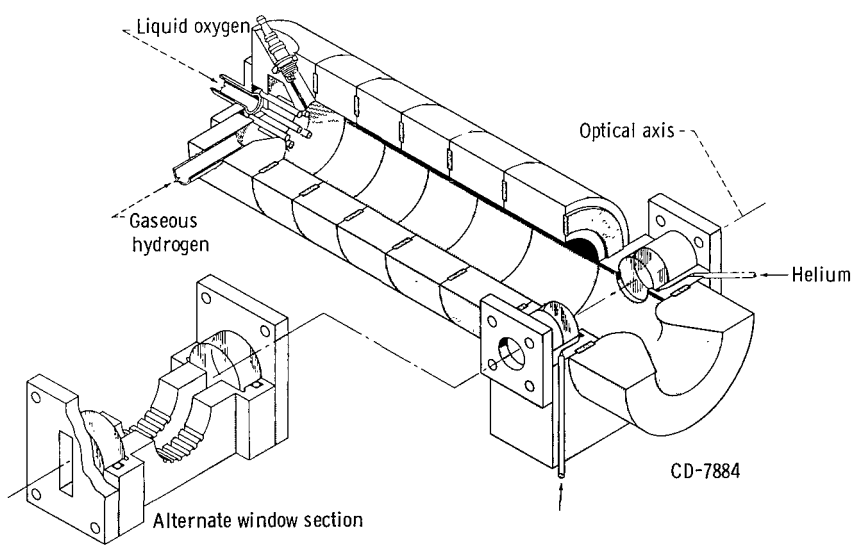

Figure 1. - Gaseous-hydrogen - liquid-oxygen combustor. Distance from injector to optical axis variable from 1.0 to 13 inches; chamber diameter, 2 inches; nozzle diameter, 0.60 inch; injector II.

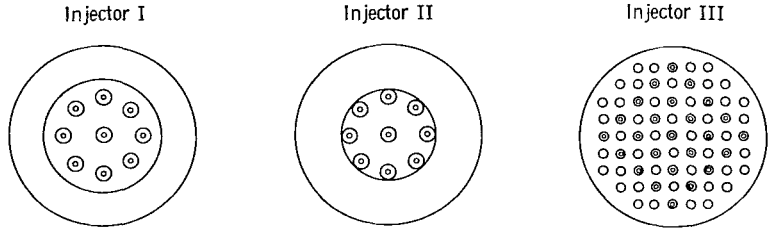

	Injector I	Injector II	Injector III
Oxygen area, sq in.	0.0072	0.0072	0.0078 (25 tubes)
Hydrogen area, sq in.	1.113	0.674	0.828 (25 concentric, 44 tubes, 0.125 in.)
Oxygen velocity, ft/sec	40 to 140	40 to 140	37 to 130
Hydrogen velocity, ft/sec	230 to 60	390 to 100	320 to 80
Percent characteristic velocity efficiency at oxidant-fuel ratio of 5	87	94	97

Figure 2. - Gaseous-hydrogen - liquid-oxygen injectors.

were used to provide low, intermediate, and high performance (fig. 2). The range of propellant velocities and typical values of the performance (percent efficiency in terms of characteristic exhaust velocity) are tabulated.

Two types of windowed sections were used to obtain emission data (fig. 1). In one, a 1-inch-diameter port provided a view along the combustor axis. In the other section, a 1/4-by 2-inch slot permitted observation of the entire chamber chamber width. A helium purge kept the quartz windows clear of solid deposits and the recessed ports free of cooler absorbing gases. The second section was also provided with grooves in the walls to hold boron nitride plates so that zones of maximum temperature could be measured. Heat transferred to these plates within the combustor caused them to sublime at temperatures higher than 3000° K.

First-surface mirrors were used to focus the ultraviolet radiation from the combustor onto the entrance slit of the spectrograph. Spectroscopic film limited the spectral range of the instrument to 2500 to 4500 angstroms in the first order of the grating and to 2500 to 3900 angstroms in the second order. Reciprocal linear dispersion on the film was 10.9 angstroms per millimeter in the first order and 5.45 angstroms per millimeter in the second order. Film exposures were 7 seconds with a 10-micron slit width and 3 seconds with a 30-micron slit width.

Spectral films were uniformly processed, and an emulsion calibration was obtained by using a stepped transmission filter and densitometer as described in appendix B. (Symbols are defined in appendix A.) Relative spectral line intensities for the various operating conditions were then determined. The procedure for determining the temperature of the radiating species from these measurements is also described in appendix B.

Total radiation intensities at each window position were recorded by a photometer with response from 2500 to 4000 angstroms. The unit consisted of an ultraviolet-sensitive photomultiplier with an S-5 response and an absorption filter. Measurements by this instrument constituted total OH, O_2, and background radiation in the ultraviolet region. Care was taken to keep the photo-

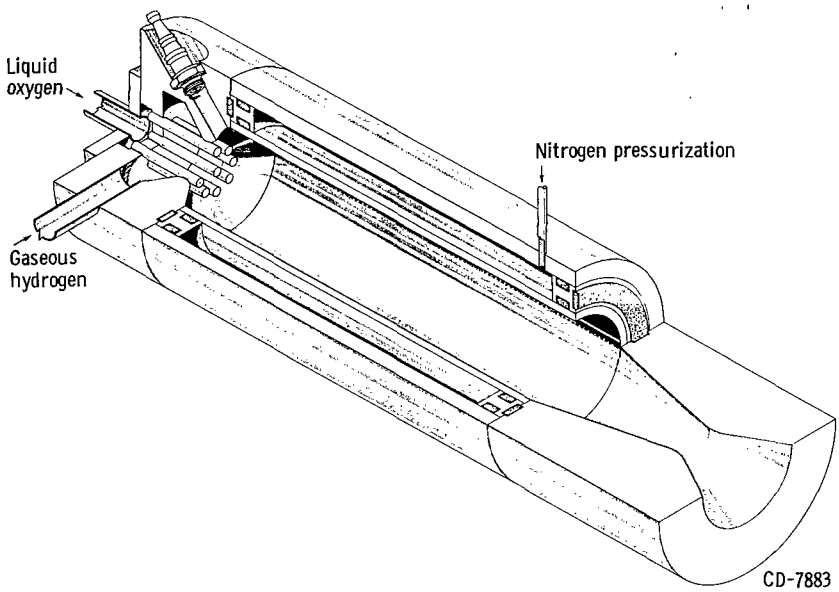

Figure 3. - Transparent combustor. Inner wall, 98 percent silica; outer wall, cast acrylic resin; diameter, 2 inches; length, 8 inches; nozzle diameter, 0.60 inch; injector II.

multiplier within its linear range and its optical path free of any absorbing gas.

Time-resolved radiation was obtained from the combustor by two methods: (1) oscilloscope records of the photometer output and (2) high-speed photographs. A special 8-inch transparent combustor (fig. 3) was used for the photographs. The transparent chamber, constructed of 98 percent silica glass and clear cast acrylic resin, transmitted radiation of wavelengths longer than 3000 angstroms; the glass optics in the camera transmitted radiation of wavelengths longer than 3100 angstroms, and thus a large portion of the OH radiation was obtained in the photographs.

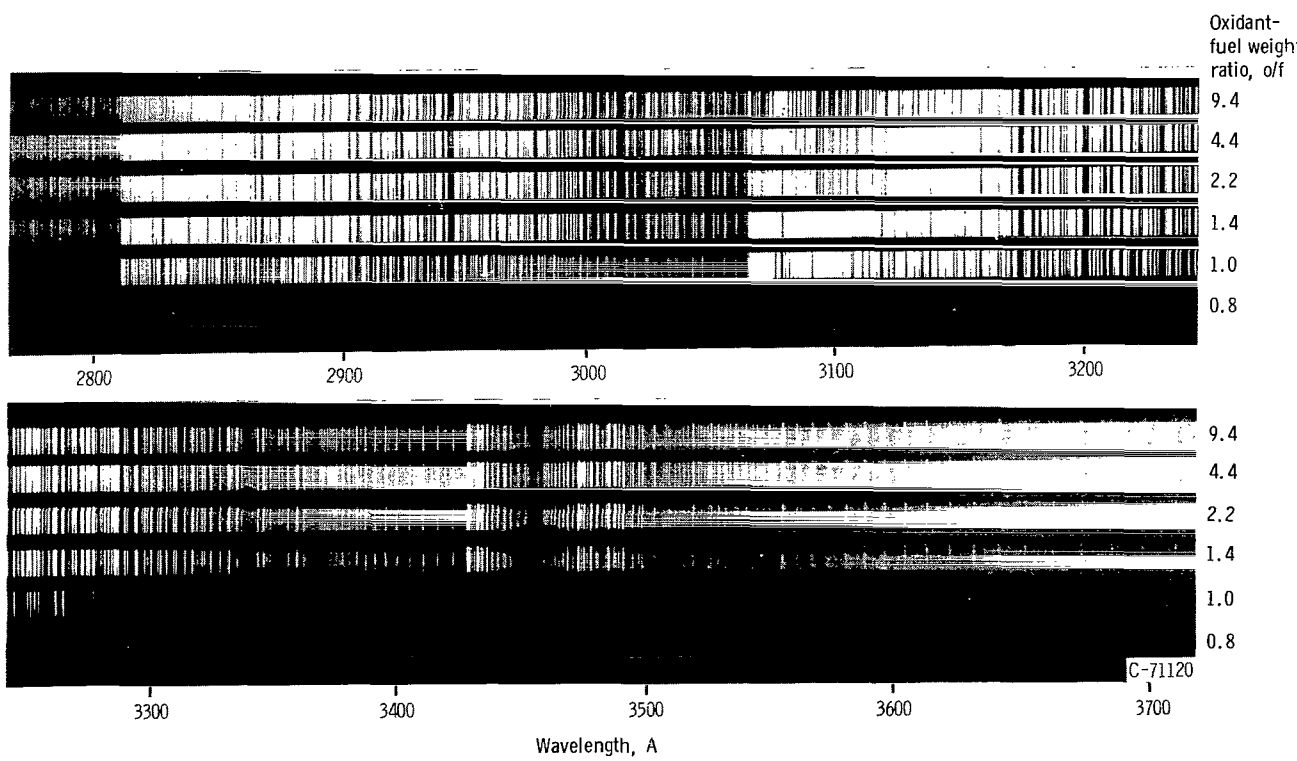

Figure 4. - Variation of radiation intensity with oxidant-fuel ratio. Pressure, 20 atmospheres; injector III; distance from injector, 1 inch.

EXPERIMENTAL RESULTS

Spectra

The spectra in figure 4 show a typical set of results in the 2800- to 3700-angstrom region. The familiar bands of OH extended from less than 2800 to more than 3500 angstroms, the much weaker Schumann-Runge system of O_2 was identified between 3000 and 4000 angstroms, and a continuum or background appeared in the entire exposed range of the film. From previous research (ref. 3), it was shown that visible radiation at wavelengths longer than 4500 angstroms was of low intensity and indicated only weak band structure.

Principal radiation was from the OH radical for all operating conditions and positions within the combustor. Oxygen line intensities increased relative to the OH line intensities with increasing oxidant-fuel weight ratio. Continuum or background radiation was proportional to the OH radiation and not the O_2 radiation for these same conditions.

Figure 5 shows the combustor flame spectrum compared with that of an atmospheric H_2-O_2 diffusion flame. The exposure time for the combustor flame spectrum was 7 seconds, and the time required to expose the same film with atmospheric flame radiation was 1 hour. The slit width was constant at 10 microns. With these exposures, strong OH lines in the combustor flame spectrum were less intense and broadened in line width compared with the same lines in the atmospheric flame. The weakest OH lines in the combustor flame spectra are more intense than the same lines in the atmospheric flame and are only slightly wider. This behavior is the same as that attributed to severe self-absorption (ref. 4). Close inspection of the (0,0) band in the spectra of figure 4 shows similar attenuation of the most intense lines, OH lines becoming reversed as oxidant-fuel weight ratio was increased. Also, intense O_2 lines became reversed near 3100 angstroms at the higher mixture ratios and hence helped to reduce the overall intensities.

(a) Pressure, 20 atmospheres.
(b) Pressure, 1 atmosphere.

Figure 5. - Comparison of hydroxyl radical spectra in (0,0) band in hydrogen-oxygen flames.

Radiating Gas Temperature

The apparent temperature of the radiating gases within the combustor was determined from two measurements, the brightness temperature of the (0,0) band of OH and the rotational temperature of the (0,1) band of OH. In the first method, the intensity of spectral lines in the 3100 angstrom region of the OH spectrum was compared photographically with the intensity of the carbon continuum emitted from the crater of a pyrometric arc operating at 3800° K. A separate experiment in which the carbon arc was viewed through the combustion zone showed almost complete absorption near 3100 angstroms; therefore, an emissivity of 1 was assumed for the gases. The crater of the carbon arc was nearly at blackbody conditions (ref. 5), and photographic spectra showed no line emission

in the 3100-angstrom region. Relative intensities of the spectra from the two alternate sources were measured on a densitometer, and the brightness temperature of the radiating gas was determined from Planck's law to be $3400^{\circ} \pm 200^{\circ}$ K. This measurement was made 6.5 inches from injector II at an oxidant-fuel ratio of 4.9 and represented nearly maximum radiation within the combustor.

Observed intensities of weak spectral lines decreased less than two orders in magnitude from their maximums when variations were made in injector type, o/f, or axial position. This represents a reduction in brightness temperature of less than 900° K. When no radiation was observed (very low o/f and large distance downstream), the brightness temperature was lower than 2500° K.

Relative rotational line intensities of the Q_1 branch in the (0,1) band of OH were measured and evaluated with regard to their rotational temperature. Details of the reasons for selecting these lines and the method of reducing the data are described in appendix B. This method yielded minimum and maximum rotational temperatures of 1640° and 3940° K for the extremes of axial position and overall o/f. The same ranges of temperatures were found regardless of axial position, o/f, or injector type. Unfortunately, a meaningful average rotational temperature could not be determined to compare with the average brightness temperature. Self-absorption and interferences of individual OH and O_2 lines prevented more accurate determinations of the rotational temperatures.

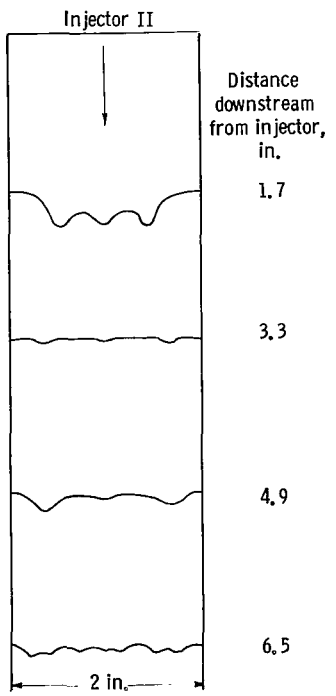

Figure 6. - Distribution of high-temperature zones in combustor as determined by erosion of boron nitride plates.

Temperature Distribution

The gas temperatures evaluated in the previous section were derived from all of the radiating zones across the diameter of the combustor. Therefore, any variation in gas temperature across the chamber would influence the average value. An estimate of the temperature distribution within the combustor was made from the erosion pattern on boron nitride plates. These plates were positioned at various axial distances from injector II and various distances from the chamber wall. The combustor was operated with an o/f of approximately 3, for which the calculated gas temperature is 2630° K. Since boron nitride sublimes at 3000° K, higher temperatures eroded the plates, and lower temperatures did not affect them. The plate profiles are shown in figure 6. Highest temperatures were consistently near or on the axes of the oxygen jets. The eroded zones expanded as the plates were positioned farther downstream, until they filled much of the combustor cross section 6.5 inches from the injector. Uneroded zones on boron nitride plates from the chamber wall to the edge of the hot gas stream were approximately 1/4 inch wide in a total gas path width of 2 inches. The modest amount of erosion at the 6.5-inch position is probably due to time-varying excursions above 3000° K.

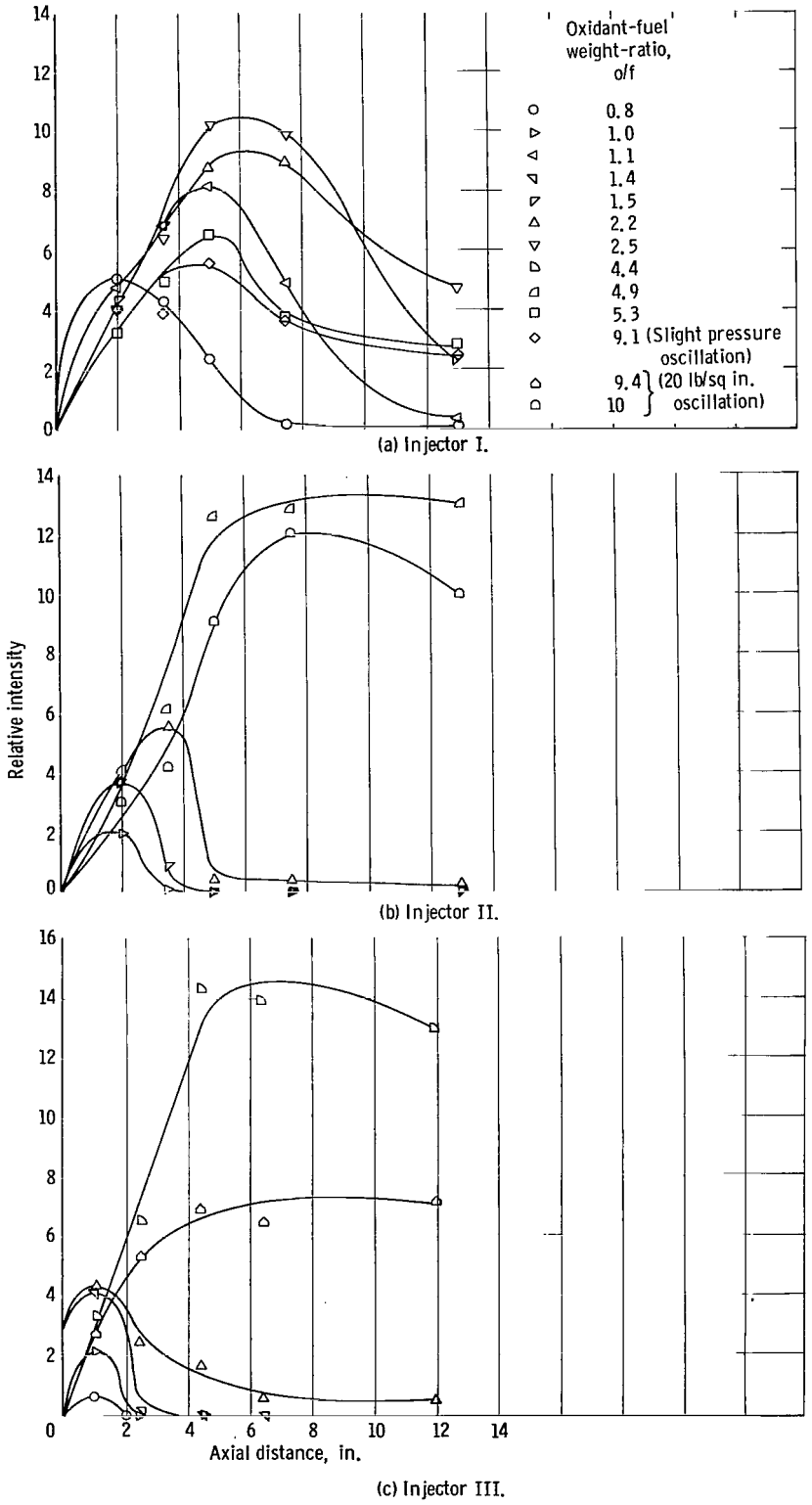

Figure 7. - Ultraviolet intensities as function of axial distance from injector.

Measured Radiation Intensities

Absolute OH intensities derived from spectrographic data varied ±50 percent for any fixed operating condition of the combustor. The difficulty was traced to variable absorption from the combustor window due to deposits and atmospheric water vapor absorption in the long optical path between the combustor and the spectrograph. Consequently, an ultraviolet photometer was used to obtain the data directly as average total intensities. Window size was reduced (to a 0.050-in.-diam.) to ensure that the window surface remained free of deposits. The optical path was flushed with dry nitrogen, and runs were repeated to assure reproducibilities of intensities within 10 percent. No attempt was made to correct the intensities for the effect of self-absorption of the OH or absorption and scattering by excess oxygen. These factors were considered characteristics of the combustion gases themselves.

Average OH intensities were obtained as a function of axial distance for three injector configurations at various oxidant-fuel ratios (fig. 7). At the low oxidant-fuel weight ratios, OH intensities reached a maximum with

increasing axial distance and then approached equilibrium values, which were sometimes below the detection limit of the photometer. At o/f values closer to stoichiometric, equilibrium radiation levels were attained with injectors II and III at the downstream position. The three injectors varied markedly in the axial positions at which both the maximum radiation and equilibrium radiation were reached for a given o/f. In general, these positions moved closer to the injector with increased injector efficiency. Thus, for an o/f of approximately 1, equilibrium OH radiation in the combustor with injector I was reached in 13 inches; with injector II, in 4 inches; and with injector III, in 3 inches. A maximum intensity of 5 was reached in 2 inches with injector I, 2 in 2 inches with injector II, and 0.7 in 1 inch with injector III.

When the more efficient injectors II and III were used on the combustor, maximum radiation from the gases was obtained at an o/f near 5, at distances more than 5 inches from the injector. Radiation intensities thereafter

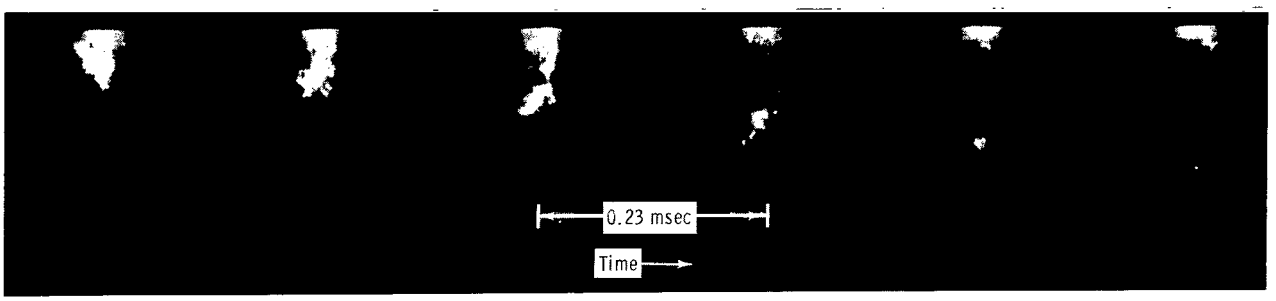

(a) Oxidant-fuel weight ratio, 1.5.

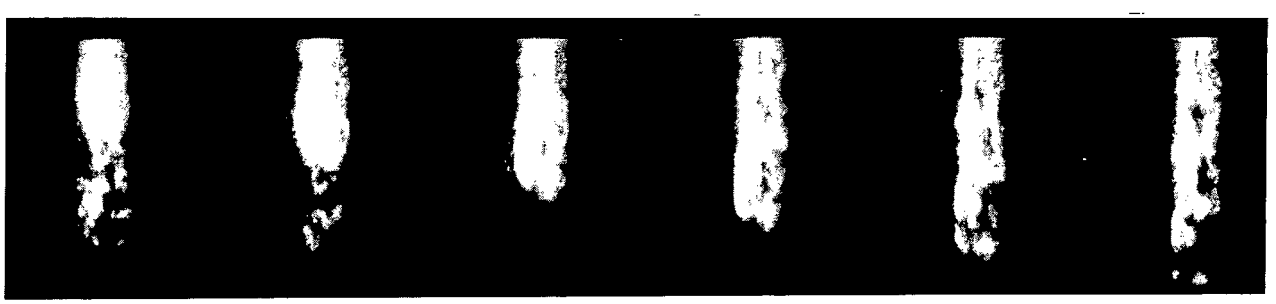

(b) Oxidant-fuel weight ratio, 2.2.

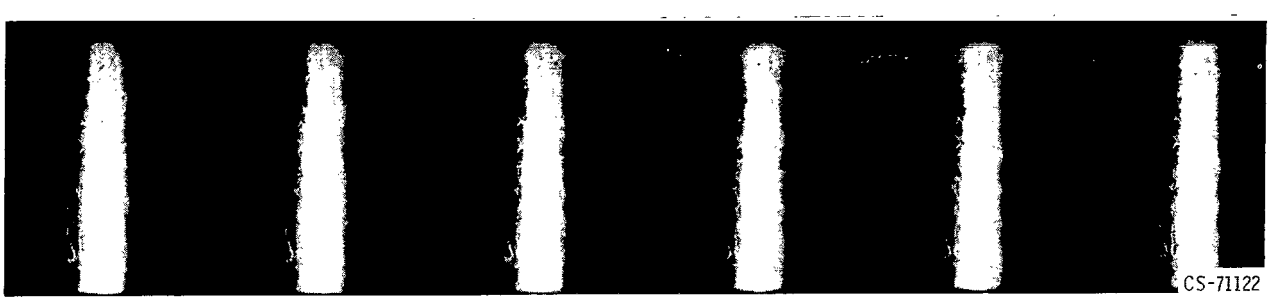

(c) Oxidant-fuel weight ratio, 10.

Figure 8. - Time resolved ultraviolet radiation as function of axial distance from injector II. Combustor diameter, 2 inches; combustor length, 8 inches.

remained nearly constant, which indicated that equilibrium intensities were nearly the same as the maximum values.

Time-varying intensities were observed in the photometer data and the high-speed photographs of the transparent chamber. Variations in radiation across the chamber and along its length are shown in figure 8. Oxidant-fuel ratios duplicate three of the settings for the photometer data in figure 7(b). The photographs show OH radiation emitted from the zones surrounding the oxygen jets. These zones extended farther downstream as the overall o/f was increased, until radiation persisted throughout the combustor length at the highest o/f setting. The sizes and intensities of the radiating zones varied, apparently because of irregularities in the oxygen flow and mixing of the products with excess propellant. However, the overall changes in time-resolved radiation with axial distance were similar to those observed for the time-averaged radiation intensities.

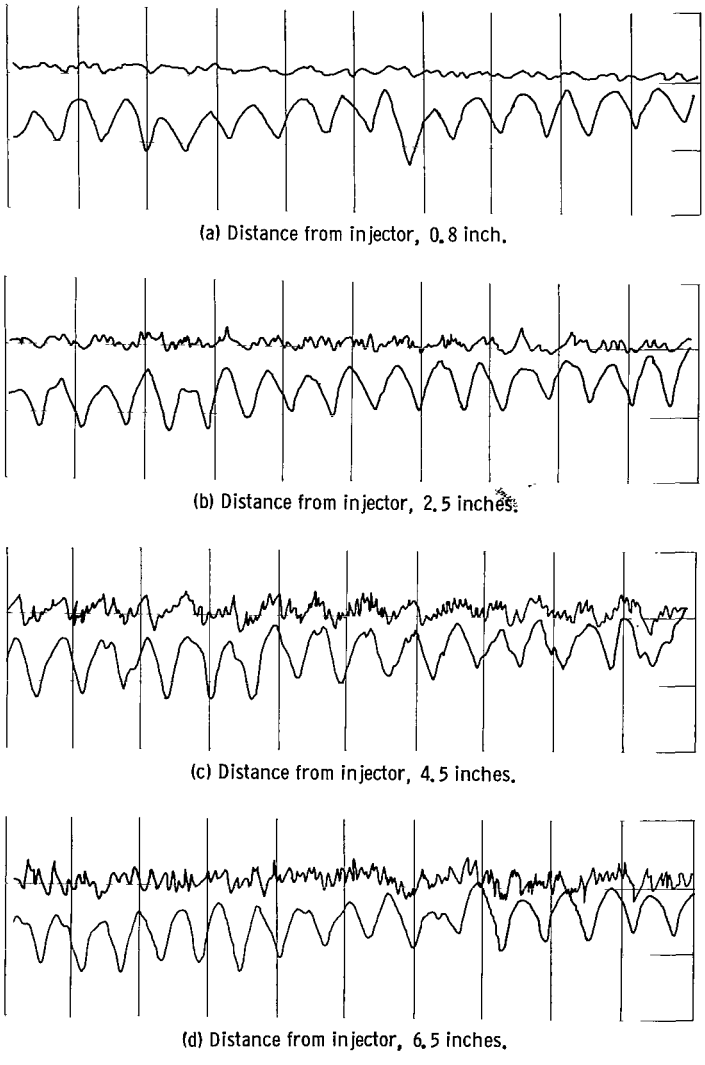

(a) Distance from injector, 0.8 inch.

(b) Distance from injector, 2.5 inches.

(c) Distance from injector, 4.5 inches.

(d) Distance from injector, 6.5 inches.

Figure 9. - Time-resolved variations in radiation intensity and chamber pressure, injector III. Frequency of pressure oscillations, 160 cps. Top trace in each figure ±12-percent variation in radiation; bottom trace in each figure ±10 psi variation in chamber pressure.

When the irregularities in the combustion become periodic, both pressure and radiation are affected. Figure 9 shows the variations in pressure and OH radiation within the combustor with injector III at an o/f of 9.4. The periodic variation in chamber pressure was approximately 20 pounds per square inch at all axial positions in the combustor at a frequency of approximately 160 cps. The OH radiation intensities appeared to be in phase with the pressure at 1, 2.5, and 4.5 inches downstream from the injector. At 6.5 inches downstream, the periodic variation in the radiation intensity was no longer present. These data were obtained at the same o/f as that used to obtain the radiation data in figure 7(c) (p. 7). In that case, the reaction was considered complete at distances from the injector greater than 6 inches.

DISCUSSION

Radiation from the reaction zone of a flame can be much stronger than that from the mixed products downstream (ref. 1). This occurs when the radiation in

the reaction zone is produced by chemiluminescent excitation or high-temperature unmixed products. The ultraviolet OH bands have occasionally shown evidence of chemiluminescent excitation, especially in low-pressure organic flames (ref. 1). This excitation is usually very weak or absent, however, when the pressure is increased above 1 atmosphere.

Hydroxyl radiation from the combustors in this study appeared to be thermally excited. The only changes observed in the relative intensities of the (1,0), (2,1), and (3,2) bands were due to self-absorption. Brightness and rotational temperatures of the OH did not greatly exceed the stoichiometric flame temperature as they do for some organic flames. It was assumed, therefore, that the OH radiation was in local equilibrium and could be used to study the extent of the H_2-O_2 reaction and subsequent mixing of the products with excess propellant.

Hydroxyl radiation that originates in gases which are in thermal equilibrium varies in intensity according to its emissivity and temperature. In the experimental data, thermal equilibrium will be approached downstream in the combustor after the combustion products are thoroughly mixed with the excess propellant. Hence, calculated OH intensities for the equilibrium gases should agree with the experimental values at this downstream position.

A simple calculation of the radiation behavior can be made by assuming that principal OH spectral lines in the (0,0) band and 3100-angstrom region have an emissivity of 1. Gas temperatures were calculated for various equilibrium mixtures of H_2 and O_2 (refs. 6 to 8) and are listed in table I. Radiation intensities determined from Planck's law vary with gas temperature and therefore with o/f as shown by the dashed curve in figure 10. Radiation data for injectors II and III showed nearly constant intensities at each o/f in the downstream positions (fig. 7). Intensities 6 to 8 inches from the injector were normalized at an o/f of 5 and also plotted in figure 10 as a function of o/f. The most significant difference between the experimental and the calculated curves is in the positions of their maximums. The theoretical curve has a sharp maximum at the stoichiometric o/f, while the experimental data from both injectors show broad maximums at fuel-rich o/f values near 5. This difference cannot be due to variations in the calculated OH concentrations, since that maximum is near an o/f of 10 (table I).

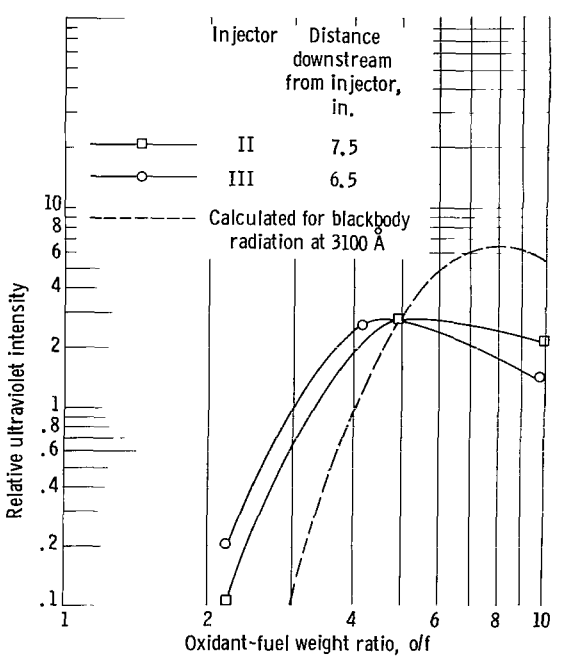

Figure 10. - Comparison of calculated and experimental equilibrium intensities as function of overall oxidant-fuel weight ratio.

It has been stated earlier that the self-absorption within the combustor was severe, especially as the overall o/f was increased. Obviously this was due in part to cool gas boundaries and in part to time

TABLE I. - EQUILIBRIUM COMBUSTOR CONDITIONS

Oxidant-fuel ratio, o/f	Equilibrium OH concentration, P_{OH}, atm (a)	Equilibrium gas temperature, T_{eq}, ^{o}K (a)	Blackbody radiance, $I_{0.31\mu}$, (w)$(cm^{-2})(\mu^{-1})$(steradian^{-1})
2	0.0002	2030	----
3	.022	2630	0.09
4	.104	3030	.97
6	1.176	3410	5.10
8	2.116	3470	6.46
10	2.382	3420	5.31
15	1.907	3190	1.25
20	1.212	2950	.61

[a]Data from refs. 6 to 8.

and spatial variations in the gases themselves. Qualitatively, then, it is possible to state that the differences between the calculated curve in figure 10 and the experimental intensities was due to self-absorption of the most intense spectral lines.

In addition, a similar shift in maximum intensities to fuel-rich o/f's can arise from space and time varying changes in the local o/f. The intensity-o/f curve is broadened in proportion to the extent of the excursion on either side of each median o/f. Calculations were made for a ±50 percent sinusoidal variation in local O_2 concentration around the values for various overall o/f's. The average radiation intensity curve for this case had a broad maximum at an overall o/f of 4.8.

It is apparent from the preceding discussion that several factors can independently change the slopes of the radiation intensity-o/f curves. Only when downstream combustor gases are completely uniform in cross section and do not vary in composition with time, will their intensity-o/f curve approach the calculated curve in figure 10.

It becomes difficult to assess the relative importance of boundary gases, concentration, and temperature on the radiation intensity when observations are made of the gases in the reaction zone. Experimental intensities in figure 7 showed two characteristics in this zone. First, since the smallest variation in radiation intensities with o/f took place near the injector, the radiation intensity must be maintained by a nearly-stoichiometric temperature zone. This behavior is similar to the behavior of laminar diffusion flames (ref. 7). Downstream radiation in the combustors increased because of increasing OH concentration and then decreased because of mixing of the products with excess hydrogen. Poor mixing and low performance greatly influenced the radiation intensities, as shown by the data for injector I. With this injector, uniform gas mixtures were not attained at the nozzle exit for most mixture ratios.

The second characteristic feature of the experimental data in figure 7 is the rapid decrease in relative intensity after maximum radiation intensities are reached at low oxidant-fuel weight ratios for injectors II and III. The axial position of maximum radiation was thus interpreted as the end of the

axial position of maximum radiation was thus interpreted as the end of the reaction zone. The data showed that the length of the reaction zone as defined increased directly with o/f and inversely with injector performance.

With efficient injectors, very short axial distances were required to establish equilibrium radiation levels. For several data points shown in figure 7, radiation decreased from a maximum level to its equilibrium level in 1.5 inches of combustor length. Assuming that the gaseous products were moving 3000 inches per second, 1.5 inches of combustor distance corresponded to 2 milliseconds. Hence, any delay of the OH radical in reaching equilibrium levels was not discernible from the data.

When periodic oscillations occurred within the combustor, the length of the reaction zone was affected. Figure 9 shows that oscillations in radiation persisted until the end of the reaction zone, after which they disappeared. Nonperiodic variations showed essentially the same characteristics in photographs of the combustors (fig. 8). All variations in the time-resolved radiation were apparently due to nonuniform propellant flows and mixing, which then appeared as localized variations in o/f.

The overall H_2-O_2 reaction in the combustor can be described on the basis of the radiation measurements presented in this work. Initially, OH intensities near the injector are nearly independent of o/f and injector efficiency. This infers that both temperature and optical depth of the OH remain nearly constant, limited to an H_2-O_2 interface nearest the observation window burning at the stoichiometric o/f. Other burning zones are blocked from view by absorption or scattering in the unburned liquid and gaseous O_2. Farther downstream, larger quantities of O_2 and H_2 react, and the effective optical depth of the OH increases, so that the radiation intensity increases faster than it can be attenuated by cool boundaries or excess propellant. Maximum intensity positions within the combustor are reached, which indicate maximum concentration of OH at nearly stoichiometric temperatures with minimum attenuation at the boundaries. Still farther downstream, the limiting propellant is consumed and the interface vanishes. The products are then mixed with the excess propellant until a homogeneous mixture is obtained, at which point the intensities approach the equilibrium levels consistent with the average thermal profile of the mixed products. Applying this model to actual combustors, radiation intensities can be used to indicate the extent of reaction and uniformity of the products as a function of distance from the injector. Hence, relative behavior of several combustor configurations can be studied on a semiquantitative basis.

SUMMARY OF RESULTS

Three combustor configurations were studied with regard to their spectral radiation behavior as a function of axial distance downstream from the injector. Results were obtained as follows:

1. The radiation from the hydroxyl radical appeared to be in thermal equilibrium with its surroundings, in both the reaction zone and in the mixed products of liquid oxygen and gaseous hydrogen at 20 atmospheres.

2. Hydroxyl and oxygen lines were subject to severe self-absorption in all the emitting bands, caused partly by the cooler boundaries near the combustor walls and partly by temperature gradients in nonuniform gas mixtures within the combustor.

3. A simple ultraviolet photometer was used to measure the relative efficiency of three injector configurations by determining the axial distance required for reaction and mixing of the products based on the equilibrium hydroxyl radiation.

4. Low-frequency periodic and nonperiodic variations in the hydroxyl radiation were interpreted as being local variations in the oxidant-fuel ratio brought about by nonuniform propellant flows or nonuniform mixing of products.

5. A description of the combustion zone based on a constant-temperature reaction with subsequent mixing of the products was consistent with the measurements.

Lewis Research Center
National Aeronautics and Space Administration
Cleveland, Ohio, September 10, 1964

APPENDIX A

SYMBOLS

A	transition probability involving vibration and rotation
a	coupling constant
c	velocity of light
E	energy of quantum state
h	Planck's constant
I	intensity of spectral line
$I_{0.31\ \mu}$	blackbody radiance, $(w)(cm^{-2})(\mu^{-1})(steradian^{-1})$
J	rotational quantum number
K	J - 1/2 for Q_1 lines
k	Boltzmann's constant, 0.967 $(cm^{-1})(^oK^{-1})$
N_o	population constant for experimental system
$N_{(v'J')}$	population of upper quantum energy state
o/f	oxidant-fuel weight ratio
P_{OH}	equilibrium OH concentration, atm
Q_1	spectroscopic symbol for particular branch of transitions
S	pure rotation transition probability
T	absolute temperature, ^oK
v	vibrational quantum number
$^2\Pi, ^2\Sigma$	electronic molecular state
ν	frequency, cm^{-1}
(0,1)	spectroscopic designation for vibrational transition between states with vibrational quantum numbers v' = 0, v'' = 1

Subscripts:

eq	equilibrium

rot rotational

Superscripts:

' upper quantum state

" lower quantum state

APPENDIX B

SUMMARY OF CALCULATIONS PERTAINING TO ROTATIONAL TEMPERATURES

The present work involved observation and interpretation of spectral intensities in the $^2\Sigma \rightarrow {}^2\Pi$ electronic transition of OH. There are several methods of interpreting such intensities to obtain temperatures of the radiating species. Briefly, this involves observations of relative intensities of the lines comprising the rotational fine structure of a vibrational branch (giving a rotational temperature), of relative vibrational band intensities (giving a vibrational temperature), and of total band radiance (giving a brightness temperature). Since thermodynamic equilibrium requires that all such temperatures agree, it is desirable to measure and compare temperatures by as many methods as possible. The results of brightness temperature measurements are given in the text. The results of the rotational temperature determination are discussed in this appendix. General treatments of the related theoretical principles of molecular quantum mechanics can be found in references 9 to 13, while details pertaining more specifically to this work are given in references 4 and 14.

Consider a collection of diatomic molecular systems in quantum energy states $E_{(v'J')}$ and $E_{(v''J'')}$, where v and J designate vibrational and rotational quantum numbers, respectively. If $E_{(v'J')}$ denotes the energy of the upper quantum state and it is assumed that there exists a temperature characteristic of a Boltzmann-like distribution, the population of the upper state $N_{(v'J')}$ is given by

$$N_{(v'J')} = N_o \exp\left[-E_{(v'J')}/kT\right] \tag{B1}$$

where N_o is a constant for the system that includes experimental factors. The intensity of a line for a transition from electronic state 1 in vibrational state v' with rotational quantum number J' to electronic state 2 in vibrational state v'' with rotational quantum number J'' is then

$$I_{(v'v''J'J'')} = N_{(v'J')} A_{(v'v''J'J'')} hc\nu \tag{B2}$$

where A is a transition probability that can be calculated theoretically. Most previous theoretical work is based on the assumption of pure rotation, that is, that the transition probability A is separable into a product of pure rotational and pure vibrational parts. The former is designated by the symbol $S_{(J'J'')}$, while the latter is usually assumed to be constant (the notation follows that employed by Learner in ref. 14).

The analysis of present experimental data involved the calculation and use of pure rotational transition probabilities for the Q_1 lines of the (0,1) vibrational branch of the $^2\Sigma \rightarrow {}^2\Pi$ transition in OH. Possible theoretical limitations of the pure rotation approach for this branch in OH have been discussed by Learner (ref. 15); however, for present purposes these did not appear to be serious. From the standpoint of background, self-absorption, and resolvability from other lines, it was found that the Q_1 lines of the (0,1) branch represent the only lines even approximately usable for analysis of OH

TABLE II. - Q_1K LINES OF (0,1) IN $^2\Sigma \rightarrow {}^2\Pi$ TRANSITION OF OH WITH INTERFERENCES

Wavelength, A	Q_1K line of OH	Relative intensity (a)	Neighboring wavelength, A	Neighboring line	Relative intensity of neighboring line (a)
3458.516	Q_11, Q_11'	(1 + 1)	--------	----------	-------
3460.051	Q_12	1	3460.118	Q_12'	0
3461.545	Q_13	2	3460.528	R_22	0
			3461.663	Q_13'	0
3463.054	Q_14	3	3462.572	P_11	1
3464.627	Q_15	3	3464.337	----------	1
			3464.768	Q_15'	0
3466.308	Q_16	3	--------	----------	-------
3468.139	Q_17	3	3468.191	P_12	1
			3468.352	----------	1
3470.132	Q_18	3	--------	----------	-------
3472.315	Q_19	3	3471.920	----------	1
			3472.038	----------	1
			3472.175	Q_23, Q_24	(2 + 2)
			3472.559	Q_25	3
			3472.705	Q_22	1
3474.704	Q_110	3	3474.441	Q_27	3
3477.307	Q_111	3	3477.567	Q_29	3
		3	3477.879	P_21'	1
3480.142	Q_112	3	3479.276	P_14	2
			3479.563	Q_210	3
			3480.887	P_22	1
3483.217	Q_113	2	3483.384	----------	1
			3483.567	Q_113'	0
			3483.736	[b] R_112, R_113	(1 + 1)
			3483.888	----------	1
3486.542	Q_114	2	3486.104	[b] R_116	0
			3486.669	----------	2
3490.134	Q_115	2	3489.970	[b] R_210	1
			3490.134	[b] R_16	1
			3490.288	[b] R_16'	0
			3490.387	Q_214	2
3494.026	Q_116	1	3493.523	----------	1
			3493.821	Q_215	2
			3494.160	[b] R_14	1

[a] Data from ref. 4.
[b] Line belongs to (1,2).

emission from the high-pressure rocket combustion gases under consideration. A detailed listing of these lines and their known interferences is given in table II.

Formulas for pure rotational transition probabilities, as derived by Hill and Van Vleck (ref. 11) and Earls (ref. 9) are given by Dieke and Crosswhite (ref. 4). For Q_1 lines the appropriate expression is

$$S(Q_1K) = \frac{2J + 1}{J(2J + 2)} \left\{ (2J + 1)^2 - 2 + \frac{(2J + 1)^3 - 8J + 2(a - 4)}{\left[(2J + 1)^2 + a(a - 4)\right]^{1/2}} \right\} \qquad (B3)$$

where a is a coupling constant whose significance is discussed in the indicated references. (Transition probabilities can be written in terms of either J' or J'', which, in a specified transition, are related through selection rules. The formulas as given in ref. 4 involve J values for the $^2\Pi$ state, i.e., J''. In the present case this becomes insignificant, however, since the Q_1 lines conform to the selection rule $J' \rightarrow J''$ (or $\Delta J = 0$). Also, transition probabilities are used with the convention of replacing J with another symbol K where for Q_1 lines $K = J - 1/2$.) Transition probabilities for the case $v'' = 0$ in the $^2\Pi$ state have been tabulated by Dieke and Crosswhite with a coupling constant $a = -7.547$. These have been recalculated here with $a = -7.876$ (see table 2 in ref. 4) for $v'' = 1$ in the $^2\Pi$ state, and are given in table III.

TABLE III. - PURE ROTATION TRANSITION PROBABILITIES

Rotation quantum number, J	$K = J - \frac{1}{2}$	2J + 1	$S(Q_1K)$ for $v'' = 1$ $a = -7.876$
$1\frac{1}{2}$	1	4	8.901
$2\frac{1}{2}$	2	6	16.84
$3\frac{1}{2}$	3	8	25.06
$4\frac{1}{2}$	4	10	33.45
$5\frac{1}{2}$	5	12	41.91
$6\frac{1}{2}$	6	14	50.37
$7\frac{1}{2}$	7	16	58.81
$8\frac{1}{2}$	8	18	67.24
$9\frac{1}{2}$	9	20	75.56
$10\frac{1}{2}$	10	22	83.86
$11\frac{1}{2}$	11	24	92.16
$12\frac{1}{2}$	12	26	100.4
$13\frac{1}{2}$	13	28	108.6
$14\frac{1}{2}$	14	30	116.8
$15\frac{1}{2}$	15	32	125.0
$16\frac{1}{2}$	16	34	133.1

These transition probabilities were used to analyze present data by a variation of the so-called fundamental method, in an effort to determine a rotational temperature for the radiating combustion gases. (Unfortunately more accurate temperature methods, such as the isointensity method, could not be used, since for $K > 8$ in the Q_1 branch of (0,1) there is serious overlap and interference from other OH lines and lines of molecular O_2.) A fundamental rotational temperature plot usually consists of a plot of

log $(I/S_{J'J''}\nu^4)$ against E_{rot}, where I is a relative intensity obtained from photographic data by a method to be explained later. If the spectrum being analyzed is from an equilibrium source that is free of self-absorption and interferences from unwanted lines, such a plot should yield a straight line whose slope is -log (e/kT). The value of k in appropriate units is k = 0.967 cm^{-1}/deg. Self-absorption will be evidenced by an "exponential" appearance of the curve for low values of K. In such a case the slope will be increased, and thus the temperature will be lower than it would be if self-absorption were absent. On the other hand, serious interference from unwanted lines at large K values (as is actually the case here) will tend to lower the slope of the plot and thus give a higher temperature than should be obtained.

Figure 11, which represents a variation of the usual rotational temperature plot, was constructed in an attempt to establish both lower and upper limits to a rotational temperature. (Energies were taken from ref. 4, table 13.) It is based on the method of choosing one line that is free of known overlap (in this case K = 6) and comparing other lines to this. Here, log $\frac{(I/S\nu^4)_{K=6}}{(I/S\nu^4)_K}$ was plotted against energy for lines K = 3, 5, 6, 8, and 13.

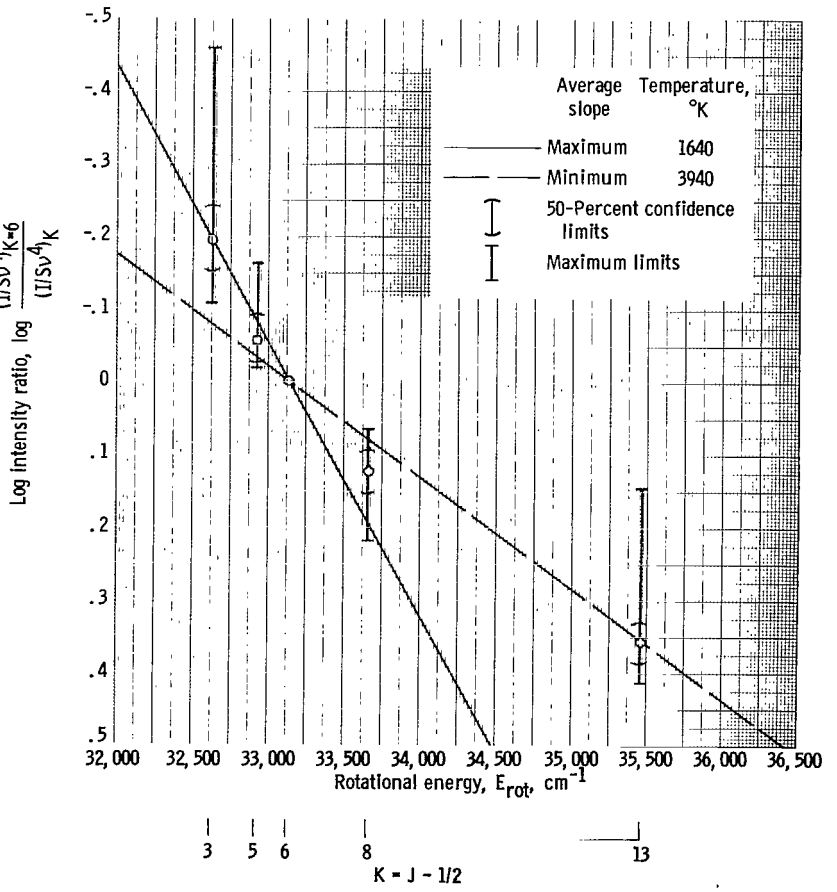

Figure 11. - Log intensity ratio as function of rotational energy for Q_1 lines of (0, 1) branch.

The first four are lines that are reasonably free from known interferences, while the last line is purposely chosen to give the effect of abnormally high intensity due to overlap from other lines. This figure represents the sum total of all data taken with all injector types used (from a total of 100 runs). About 20 percent of these data involved unusually severe self-absorption conditions, where the band head of the (0,0) branch was almost completely reversed. Consequently, the final results include the influences of self-absorption. The data points in figure 11 represent the average ratios obtained, while the ranges of variation in these ratios for all data are indicated by both maximum limits and 50-percent confidence limits. The latter represent

the range of values represented by 50 to 70 percent of the data. Maximum and minimum "average slopes" are shown through the points representing ratio averages. The former indicate a minimum average temperature of 1640° K, while the latter represent a temperature of 3940° K.

Although the maximum and minimum rotational temperatures differed by 2300° K, this does not imply that the true average temperature varied throughout this range. First, neighboring line interferences increased line intensities at high K values and caused the maximum rotational temperature to be too high. Second, self-absorption increased the slope at low K values and caused the minimum rotational temperature to be too low. Photographic intensities in this work were all within a single order of magnitude (1.43 to 8.00). This range in intensities corresponds to a similar range in concentration or an OH temperature range of less than 500° K according to equation (B2). It is improbable that the OH concentration will decrease with increasing temperature so that observed intensities could correspond to the wide temperature range of 1640° to 3940° K. Thus the true range in OH temperatures must be within much narrower limits than indicated by the rotational temperatures. Since the brightness temperature of the OH was 3400°±200° K, it is probable that the rotational temperatures were within the same range. Unfortunately an average rotational temperature cannot be determined from the data to compare with the brightness temperature. (From a consideration of the theory related to the (0,1) branch (ref. 14), it is probable that marked nonequilibrium would appear in this branch. Since the upper rotational temperature limit is not excessive, it can be inferred that any departure from equilibrium, if it exists, is not serious in this work.)

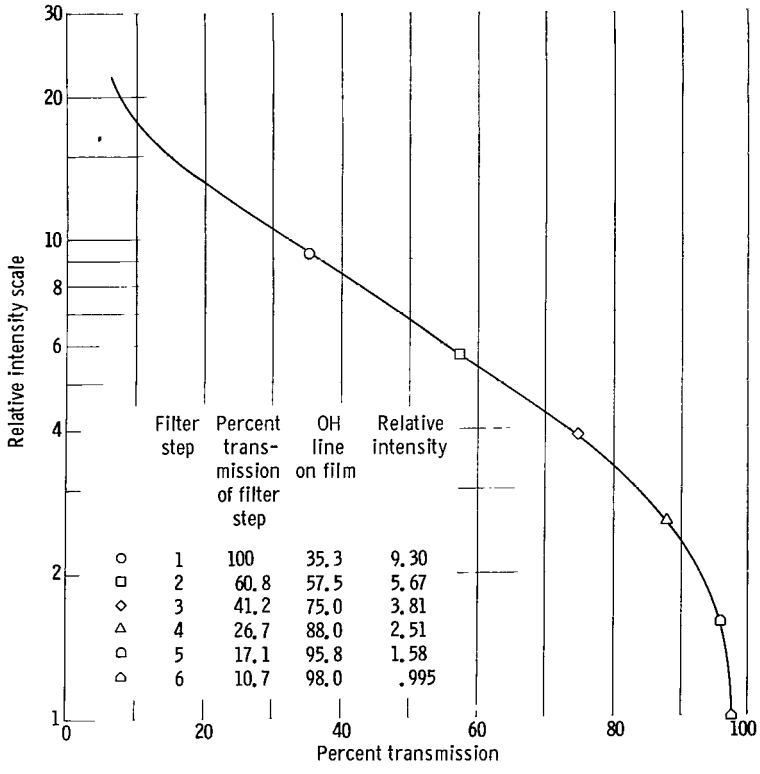

Figure 12. - Film transmission as function of source intensity. Wavelength, 3500 Å.

The preceding analysis required comparing one line to another on a (relative) intensity scale that is related to the percent transmission of a film line as read from a densitometer. (Percent transmission is relative to a 100-percent level defined by a clear portion of the photographic emulsion and a 0-percent level defined by a closed densitometer slit.) The intensity scale is given by an emulsion calibration (fig. 12) constructed according to the step filter method discussed by several authors (ref. 15 and 16). In this case spectra were taken by using a seven step multiple density

filter with step transmissions of 100 percent (clear filter), 60.8, 41.2, 26.7, 17.1, 10.7, and 6.7 percent. This yielded a spectral line whose total line height on the photographic emulsion was divided into seven intensity regions. The percent film transmission of the most intense region was set equal to an arbitrary intensity level (about 10). Since the unfiltered light all corresponded to the same actual spectral source intensity, the percent film transmission of the next step corresponded to an intensity level 0.608 of 10, or 6.08, and so forth. The curve in figure 12 was constructed from a composite of data taken from OH and carbon arc light sources in the wavelength range covered by the (0,1) branch in OH. Data points obtained from a typical line are located on this curve in order to illustrate the method of constructing a calibration.

Lewis Research Center,
National Aeronautics and Space Administration,
September 1, 1964.

REFERENCES

1. Gaydon, A. G.: The Spectroscopy of Flames. John Wiley & Sons, Inc., 1957.

2. Gaydon, A. G., and Wolfhard, H. G.: Flames, Their Structure, Radiation, and Temperature. Second ed., rev., Chapman & Hall, London, 1960.

3. Burrows, Marshall C., and Povinelli, Louis A.: Emission Spectra from High-Pressure Hydrogen-Oxygen Combustion. NASA TN D-1305, 1962.

4. Dieke, G. H., and Crosswhite, H. M.: The Ultraviolet Bands of OH Fundamental Data. Jour. Quant. Spectroscopy Radiation Transfer, vol. 2, Apr-June 1962, pp. 97-199.

5. Null, M. R., and Lozier, W. W.: The Carbon Arc as a Radiation Standard. Temperature; Its Measurement and Control in Science and Industry, 1961.

6. Zeleznik, Frank J., and Gordon, Sanford: A General IBM 704 or 7090 Computer Program for Computation of Chemical Equilibrium Compositions, Rocket Performance, and Chapman-Jouguet Detonations. NASA TN D-1454, 1962.

7. Gordon, Sanford, and Zeleznik, Frank J.: A General IBM 704 or 7090 Computer Program for Computation of Chemical Equilibrium Compositions, Rocket Performance, and Chapman-Jouguet Detonations - Supplement 1 - Assigned Area-Ratio Performance. NASA TN D-1737, 1963.

8. McBride, Bonnie J., Heimel, Sheldon, Ehlers, Janet G., and Gordon, Sanford: Thermodynamic Properties to 6000° K for 210 Substances Involving the First 18 Elements. NASA SP-3001, 1963.

9. Earls, L. T.: Intensities in $^2\Pi - {}^2\Sigma$ Transitions in Diatomic Molecules. Phys. Rev., vol. 48, no. 5, Sept. 1, 1935, pp. 423-424.

10. Eyring, H., Walter, J., and Kimball, G. E.: Quantum Chemistry. John Wiley & Sons, Inc., 1944.

11. Hill, E., and Van Vleck, J. H.: On the Quantum Mechanics of the Rotational Distortion of Multiplets in Molecular Spectra. Phy. Rev., vol. 32, no. 2, Aug. 1928, pp. 250-272.

12. Landau, L. D., and Lifshitz, E. M.: Quantum Mechanics - Nonrelativistic Theory. Addison-Wesley Pub. Co., Inc., 1958.

13. Pekeris, C. L.: The Rotation-Vibration Coupling in Diatomic Molecules. Phy. Rev., vol. 45, no. 2, Jan. 15, 1934, pp. 98-103.

14. Learner, R. C. M.: The Influence of Vibration-Rotation Interaction on Intensities in the Electronic Spectra of Diatomic Molecules. I. The Hydroxyl Radical. Proc. Roy. Soc. (London), ser. A, vol. 269, no. 1338, Sept. 25, 1962, pp. 311-326.

15. Brode, Wallace Reed: Chemical Spectroscopy. John Wiley & Sons, Inc., 1939.

16. Harvey, C. E.: Spectrochemical Procedures. Appl. Res. Lab., 1950.

"The aeronautical and space activities of the United States shall be conducted so as to contribute . . . to the expansion of human knowledge of phenomena in the atmosphere and space. The Administration shall provide for the widest practicable and appropriate dissemination of information concerning its activities and the results thereof."

—NATIONAL AERONAUTICS AND SPACE ACT OF 1958

NASA SCIENTIFIC AND TECHNICAL PUBLICATIONS

TECHNICAL REPORTS: Scientific and technical information considered important, complete, and a lasting contribution to existing knowledge.

TECHNICAL NOTES: Information less broad in scope but nevertheless of importance as a contribution to existing knowledge.

TECHNICAL MEMORANDUMS: Information receiving limited distribution because of preliminary data, security classification, or other reasons.

CONTRACTOR REPORTS: Technical information generated in connection with a NASA contract or grant and released under NASA auspices.

TECHNICAL TRANSLATIONS: Information published in a foreign language considered to merit NASA distribution in English.

TECHNICAL REPRINTS: Information derived from NASA activities and initially published in the form of journal articles.

SPECIAL PUBLICATIONS: Information derived from or of value to NASA activities but not necessarily reporting the results of individual NASA-programmed scientific efforts. Publications include conference proceedings, monographs, data compilations, handbooks, sourcebooks, and special bibliographies.

Details on the availability of these publications may be obtained from:

SCIENTIFIC AND TECHNICAL INFORMATION DIVISION

NATIONAL AERONAUTICS AND SPACE ADMINISTRATION

Washington, D.C. 20546